Contribution of Kv1.2 Voltage-gated Potassium Channel to D2 Autoreceptor Regulation of Axonal Dopamine Overflow*[S]

Stephanie Fulton[‡1], **Dominic Thibault**[‡], **Jose A. Mendez**[‡], **Nicolas Lahaie**[§], **Emanuele Tirotta**[¶], **Emiliana Borrelli**[¶], **Michel Bouvier**[§2], **Bruce L. Tempel**[||], **and Louis-Eric Trudeau**[‡3]

From the [‡]Department of Pharmacology and Groupe de Recherche sur le Système Nerveux Central, and the [§]Institute for Research in Immunology and Cancer and Department of Biochemistry, Université de Montréal, Quebec H3C 3J7, Canada, the [¶]Department of Microbiology and Molecular Genetics, University of California, Irvine, California 92617, and the Departments of [||]Otolaryngology and Pharmacology, University of Washington, Seattle, Washington 98915

Impairments in axonal dopamine release are associated with neurological disorders such as schizophrenia and attention deficit hyperactivity disorder and pathophysiological conditions promoting drug abuse and obesity. The D2 dopamine autoreceptor (D2-AR) exerts tight regulatory control of axonal dopamine (DA) release through a mechanism suggested to involve K$^+$ channels. To evaluate the contribution of Kv1 voltage-gated potassium channels of the *Shaker* gene family to the regulation of axonal DA release by the D2-AR, the present study employed expression analyses, real time measurements of striatal DA overflow, K$^+$ current measurements and immunoprecipitation assays. *Kv1.1, -1.2, -1.3,* and *-1.6* mRNA and protein were detected in midbrain DA neurons purified by fluorescence-activated cell sorting and in primary DA neuron cultures. In addition, Kv1.1, -1.2, and -1.6 were localized to DA axonal processes in the dorsal striatum. By means of fast scan cyclic voltammetry in striatal slice preparations, we found that the inhibition of stimulation-evoked DA overflow by a D2 agonist was attenuated by Kv1.1, -1.2, and -1.6 toxin blockers. A particular role for the Kv1.2 subunit in the process whereby axonal D2-AR inhibits DA overflow was established with the use of a selective Kv1.2 blocker and Kv1.2 knock-out mice. Moreover, we demonstrate the ability of D2-AR activation to increase Kv1.2 currents in co-transfected cells and its reliance on G$\beta\gamma$ subunit signaling along with the physical coupling of D2-AR and Kv1.2-containing channels in striatal tissue. These findings underline the contribution of Kv1.2 in the regulation of nigrostriatal DA release by the D2-AR and thereby offer a novel mechanism by which DA release is regulated.

Dopamine (DA)[4] neurons originating in the midbrain ventral tegmental area and substantia nigra and projecting to limbic and cortical sites are important for motor control, motivation, and cognition, and impairment in their function contributes to neurological and behavioral disorders. Diminished striatal DA concentrations are linked to drug abuse, overeating, and obesity (1–3), whereas the pattern of DA neurotransmission is critical for encoding the predictability and salience of rewarding stimuli (4–6). The dynamics of DA release in mesolimbic and nigrostriatal pathways are regulated in part by D2-autoreceptors (D2-AR). Located on somatodendritic and axonal compartments of DA neurons, the D2-AR provides negative feedback by rapidly inhibiting DA release (7). At the somatodendritic level, D2-AR opens type-2 G-protein gated inward-rectifying K$^+$ channels (GIRK-2) to reduce DA neuron firing (8, 9), however, little is known about the mechanisms linking axonal D2-AR activation to reduced DA release.

The D2-AR belongs to the D2-like family of G-protein coupled receptors that inhibit adenylate cyclase via G$_{i/o}$. The short splice variant of the D2 receptor (D2S), acting as the presynaptic D2-AR, is both molecularly and functionally distinct from its postsynaptic, long isoform (D2L) (10–12). It has been proposed that the D2-AR inhibits DA release by increasing potassium conductance (13, 14). The somatodendritic D2-AR directly couples to G-protein gated inward-rectifying K$^+$ channels via G-protein $\beta\gamma$ subunits (15). In contrast, the axonal D2-AR appears to diminish DA release via the opening of unidentified voltage-gated K$^+$ channels (14, 16).

Voltage-dependent K$^+$ channels play a fundamental role in the generation of action potentials and in regulating neuronal excitability. In addition, Kv1-family members have been shown to be present on axon terminals and to regulate neurotransmitter release (16–20). Kv1 channels of the *Shaker* gene family consist of eight members of which Kv1.1 through 1.6 α subunits are expressed in the mammalian brain (19, 21, 22). The Kv1 channel pore is composed of four α subunits that can co-assem-

[4] The abbreviations used are: DA, dopamine; D2-AR, D2-autoreceptors; TH, tyrosine hydroxylase; P0, postnatal day 0; SN, substantia nigra; VTA, ventral tegmental area; DAT, dopamine transporter; 4-AP, 4-aminopyridine; αDTX, α-dendrotoxin; IP, immunoprecipitation; NEM, *N*-ethylmalemide; ANOVA, analysis of variance; MTX, maurotoxin; GAD, glutamic acid decarboxylase; TAT, transactivator of transcription; KO, knockout; GRKct, G protein-coupled receptor kinase carboxyl terminus.

ble in different combinations to form an array of heteromultimeric channels (23, 24). The present work identifies the contribution of Kv1.1, -1.2, and -1.6 subunit-containing channels in the dorsolateral striatum by means of mRNA and protein expression analyses as well as real time measurements of axonal DA overflow using cyclic voltammetry during perfusions of novel Kv1 toxin blockers. We establish a particular role for Kv1.2 in the process whereby axonal D2-AR inhibits DA overflow in studies employing a toxin blocker selective for the Kv1.2 subunit and Kv1.2 knock-out mice, and by demonstrating functional and physical coupling between D2-AR and Kv1.2.

EXPERIMENTAL PROCEDURES

Subjects—A transgenic mouse line in which the *tyrosine hydroxylase* (TH) promoter drives green fluorescent protein expression (TH-eGFP/21–31) on a C57BL/6 background was used for most experiments. TH-eGFP mice between the ages of P0−1 or P25−35 days were used for DA cultures and fluorescent-activated cell sorting, respectively. Male TH-eGFP heterozygous mice or wild type littermates, 4 to 6 weeks of age, were used for slice immunohistochemistry and cyclic voltammetry experiments. For the remaining cyclic voltammetry experiments, male Kv1.2 knock-out mice (Kcna2^{tm1Tem}, referred to here as Kv1.2$^{-/-}$) and wild type littermates (Kv1.2$^{+/+}$) on a C3HeB/FeJ background were used. Kv1.2$^{-/-}$ mice completely lacking Kv1.2 channel subunit protein have increased seizure susceptibility and reduced lifespan (mean age = 17 ± 0.2 days) and thus were used between the ages of P15 and 17 (25). For immunoprecipitation experiments we used adult D2 knock-out (26), D2L knock-out (11), and wild type mice littermates on a C57BL/6 background. Genotyping for TH-eGFP and Kv1.2$^{-/-,+/+}$ mice was performed on tail DNA according to published protocols (25, 27). All procedures involving the use of animals were approved by the Université de Montréal Animal Ethics Committee and are in accordance with the guidelines on the care and use of experimental animals outlined by the Canadian Council on Animal Care.

Fluorescent-activated Cell Sorting—TH-eGFP mice (25–35 days old) were anesthetized with halothane and decapitated. Cubes of tissue containing the substantia nigra (SN) and ventral tegmental area (VTA) were dissected from 2 to 3 mice for each FACS sample. The tissue treatment and cell dissociation procedures used have been described elsewhere (27). Cell suspensions were sorted using a BD FACSAria flow cytometer (BD BioSciences) according to GFP fluorescence profiles. The threshold for GFP detection was set beforehand according to cell suspensions derived from wild type mice.

Multiplex PCR—Total RNA was isolated from FACS-purified cells and brain tissue controls using TRIzol (Invitrogen). PCR were performed using 20% of the RT reaction, 1.5 mM MgCl$_2$, 0.5 mM dNTPs mixture, 10 pmol of each primer (see below), 5 units of *Taq* DNA polymerase (Qiagen) in PCR buffer (20 mM Tris-HCl, 50 mM KCl, pH 8.3). Multiplex PCR were resolved in 1.5% agarose gels and imaged on a Kodak DC290 system. Multiplex PCR and electrophoresis on cDNA derived from FACS-purified cells was performed five times using separate samples.

Primers—All primers were designed according to sequences deposited in the GenBank^{TM} data base using Vector NTI and MultAlin multiple sequence alignment (28) software and synthesized by AlphaDNA (Montreal, QC, Canada). All primers were tested using the appropriate positive controls. A combination of primers to perform multiplex PCR was established by their ability to not interact with other primers and PCR product size. Right primers are followed by left primers: Kv1.1, 5′-ggccatcatccccttatttca-3′ and 5′-gctcttcccccctcagtttct-3′; Kv1.2, 5′-ctatgacccagaggcagacc-3′ and 5′-tcatcctcccgaaacatctc-3′; Kv1.3, 5′-atgcacccagtgaccatagg-3′ and 5′-gctgaagaggagaggtgctg-3′; Kv1.4, 5′-gaagtggcgatggtgagtg-3′ and 5′-aggtctgagcaatgaggaaaac-3′; Kv1.5, 5′-cgacggctggactcaataa-3′ and 5′-atgaccaagaccgacacga-3′; Kv1.6, 5′-cgaggaagaagatgaggatga-3′ and 5′-ccgtctctcggtggtagaagt-3′; Kv.4.2, 5′-tctgatagtgctgaacgtgagtg-3′ and 5′-cacaaggcagttcttttatgtgg-3′; TH, 5′-gtacaaaaccctcctcactgtctc-3′ and 5′-cttgtattggaaggcaatctctg-3′; GAD-67, 5′-atatcattggtttagctggtgaatg-3′ and 5′-gtgactgtgttctgaggtgaagag-3′.

Immunocytochemistry—Primary cultures of midbrain DA neurons were prepared from TH-eGFP reporter mice and maintained as described elsewhere (29, 30). Standard DA neuron cultures, 10−17 days old, were fixed with 10% buffered formalin (Sigma), blocked in 5% normal goat serum with 0.1% Triton and 0.02% NaN$_3$. Double immunofluorescence was performed with antibodies directed against the dopamine transporter (DAT) (1:1000; Chemicon) and Kv1.1 through 1.6 (1:1000; Neuromab), and visualized using Alexa Fluor-coupled secondary antibodies, 488 for DAT and 647 for Kv1 (1:200; Molecular Probes). Three to four coverslips were processed per Kv1 subtype. Coverslips without primary antibody served as controls.

Immunohistochemistry—Four male mice were anesthetized with pentobarbital (150 mg/kg) and perfused transcardially with ice-cold saline followed by 10% buffered formalin. Brains were removed and post-fixed in 10% buffered formalin for 8−12 h. Coronal brain sections were sliced at 30 μm throughout the rostrocaudal extent of the striatum using a vibrating microtome (Leica VT1000S) and collected in four series. Each slice series was subject to double immunofluorescence using antibodies against DAT (1:1000; Chemicon) and Kv1.1, Kv1.2, Kv1.3, or Kv1.6 (1:1000; Neuromab). Fluorescent detection was performed using Alexa Fluor-coupled secondary antibodies (1:200; Invitrogen). Slices without primary antibody served as controls.

Confocal Microscopy—All images were captured with a point-scanning confocal microscope (Prairie Technologies, Middleton, WI) equipped with an argon (wavelength 488 nm) and helium/neon (633 nm) laser. For the analysis of Kv1.x and DAT co-localization, all image acquisition parameters were kept constant across Kv1 subtypes. For colocalization analyses in striatal slices, confocal images of the dorsal striatum were acquired from two pre-selected rostrocaudal levels: 1) +1.10 − 1.34 and 2) 1.42–1.54 mm from bregma. Z-stack confocal images were acquired at 1-μm intervals and 10−15 images were acquired per stack. Co-localization analyses were performed on 5 images derived from the middle of each Z-stack series. Using ImageJ software (31), DAT and Kv1.x signal thresholds were set according to negative (no primary antibody) controls. To

obtain the colocalization signal values we used the *colocalize* function of ImageJ (additional *Plugin*), which isolates the overlapping signals. Colocalized images and DAT alone images were then thresholded using ImageJ (*Image − Adjust*) to create binary images. Particles in each DAT and DAT + Kv1 binary image were measured using the *Analyze Particles* command. This analysis generated values for the total signal area of DAT and Kv1.x+DAT colocalization. Values were obtained for each of the 5 stacked images and then averaged. Values representing the proportion of total DAT signal area occupied by Kv1.x were calculated (signal area of Kv1.x + DAT/DAT).

Drugs and Toxins—Quinpirole, 4-aminopyridine (4-AP), *N*-ethylmaleimide (NEM), and all chemicals were purchased from Sigma. Peptide toxins were purchased from Alomone Labs (Jerusalem, Israel). Lyophilized toxins were dissolved as stock solutions in 0.1% BSA, 100 mM NaCl, 10 mM Tris (pH 7.4).

Fast Scan Cyclic Voltammetry—Mice were anesthetized with halothane prior to decapitation. Coronal slices, 300-μm thick, were cut using a vibratome at the level of the dorsal striatum (+1.10−1.70 mm from Bregma) in ice-cold carbogenated artificial cerebrospinal fluid (ACSF) containing 125 mM NaCl, 26 mM NaHCO$_3$, 2.5 mM KCl, 2.4 mM CaCl$_2$, 1.3 mM MgSO$_4$, 0.3 mM KH$_2$PO$_4$, and 10 mM D-glucose. Slices were cut in half and maintained in carbogenated ACSF at room temperature for at least 1 h prior to recordings. Once in the recording chamber, slices were superfused with ACSF maintained at 32 °C at a rate of 1 ml/min. Carbon-fiber electrodes were constructed according to procedures described elsewhere (32) and were cut to obtain basal currents between 100 and 180 nA. To promote greater sensitivity, electrodes were soaked in carbon-purified isopropyl alcohol for at least 10 min before use (33). Electrodes were calibrated *in vitro* using known concentrations of DA. The carbon fiber electrode was positioned in the dorsolateral striatum, $\sim$100 μm into the slice and $\sim$100 μm from the center of the tips of a bipolar stimulating electrode that rested on the surface of the slice. Upon positioning the stimulation and carbon fiber electrodes in the dorsolateral striatum, slices were left to stabilize for 20 min before electrochemical recordings. One recording and stimulation site per slice was tested and each slice served as its own precondition control. Fast scan cyclic voltammetry was used to measure electrically evoked DA overflow (34, 35). The potential of the carbon fiber electrode was held at −0.4 V *versus* Ag/AgCl between scans and was linearly ramped from −0.4 to +1.0 V and then back to −0.4 V at a rate of 300 V/s. Each triangular waveform scan lasted 10 ms and was repeated every 100 ms. Data acquisition was carried out with an Axopatch 200B amplifier (Axon Instruments) connected to a Compaq Pentium III computer and pClamp 9 software through a DigiData 1200B analog to digital interface (Molecular Devices). DA overflow was evoked at 2-min intervals by a single 400-μA rectangular electrical pulse (1 ms) delivered by an S-900 stimulator (Dagan Corporation, Minneapolis, MN) through a bipolar stimulating electrode (Plastics One, Roanoke, VI). Background current waveforms obtained immediately before the stimulation were subtracted from current waveforms obtained after stimulation to generate DA cyclic voltammograms (Fig. 4*A*). Current waveforms remained stable over the course of testing. Oxidation current peaks for DA were

obtained at potentials of $\sim$300 –500 mV (*versus* Ag/AgCl) corresponding to 3.5– 4.5 ms in the voltage waveform (Fig. 4*A*).

Statistical Analyses—The peak oxidation currents derived from voltammograms were converted to concentration by electrode calibration and used to generate current-time plots (Fig. 4*B*). Each slice served as its own precondition control, thus maximal DA concentrations (Fig. 4*B*) were normalized to a respective baseline period: the 8-min period immediately prior to drug or toxin application. Drugs and toxins were applied until maximal effects on DA overflow were observed, ranging between 15 and 30 min, with the exception of quinpirole, which was applied for 4 min. Thus, the effect of a drug/toxin on evoked DA overflow was evaluated during a period after which stable effects were achieved, represented by the last 8 min of drug/toxin application. Mean values from this 8-min period were used for statistical comparisons. The ability of quinpirole to inhibit DA overflow was determined at its peak effect. The effect of drug/toxin alone on DA overflow was assessed by comparing to overflow values obtained in separate slices perfused with ACSF alone for the same duration (basal overflow). Similarly, the influence of drug/toxin preincubation on the inhibitory effects of quinpirole on DA overflow was assessed by comparing to separate slices in which quinpirole alone was applied 30 min after the baseline control period (*i.e.* the same duration that drug/toxin was applied). The influence of 4-AP on DA was assessed using an unpaired t test. The remaining drug and toxin analyses were carried out using a one-way ANOVA and Dunnett test for multiple comparisons. DA overflow in slices derived from Kv1.2$^{-/-}$ mice and wild type littermates (Kv1.2$^{+/+}$) were evaluated by unpaired t tests. To evaluate the influence of TAT-GRK peptides on DA overflow, a one-way ANOVA with a Newman-Keuls test was used. Values that met Chauvenet's criterion for statistical outliers (>2 standard deviations) were excluded (6 of a total of 129 values). All data are shown as mean $\pm$ S.E. The sample size is indicated as $n = (x;y)$, x referring to the number of slices and y the number of mice. An α level of $p \leq 0.05$ was set as the criterion for statistical significance.

Transactivator of Transcription (TAT)-G Protein-coupled Receptor Kinase-Carboxyl Terminus (GRKct) Peptide Construction and Validation—See supplemental "Experimental Procedures."

Kv1.2 and D2-AR Transfections for K$^+$ Current Measurements—HEK293 cells were plated on collagen/poly-L-lysine precoated 1.5-cm round glass coverslips and incubated in 100 $\times$ 15-mm Petri dishes (2 coverslips per dish) containing 2.5 ml of DMEM enriched with 1% penicillin-streptomycin, 1% glutamine, and 10% FBS. Upon reaching $\pm$80% confluence, the coverslips were transferred to 12-well plates containing 1 ml/well of basic DMEM, and the cells were transiently co-transfected with *Kv1.2-YFP* and *D2S-myc* or *D2L-myc* plasmids or *Kv1.2-YFP + D2S-myc* (or the FLAG epitope for immunocytochemistry) + *GRKct-myc* (36) plasmids (in the case of triple transfections) using Lipofectamine (Invitrogen) according to the manufacturer's instructions. The coverslips were inserted in a recording chamber affixed to the stage of an inverted Nikon Eclipse TE-200 fluorescent microscope and gravitationally perfused with saline. Whole cell patch clamp recordings were performed on YFP (Kv1.2) express-

ing cells using borosilicate pipettes (5.5–6.5 MΩ) filled with an intra-pipette solution composed of (in mM): KMeSO$_4$, 145; KCl, 20; NaCl, 10; EGTA, 0.1; ATP (Mg salt), 2; GTP (Tris salt), 0.6; HEPES, 10; phosphocreatine, 10 (pH 7.35). The signal was amplified by a Warner PC-505 amplifier, filtered at 1 kHz, digitized at 10 kHz, and analyzed with pClamp8 software (Molecular Devices). Series resistance was in the range of 10 MΩ and was compensated to ~75%. Membrane voltage was stepped sequentially from −80 to +30 mV using 200-ms depolarizing steps and leak-subtracted membrane currents were recorded at a rate of one series per minute. K$^+$ current amplitudes were normalized by cell capacitance. As a control, K$^+$ currents were also recorded in non-transfected cells. Quinpirole (1 μM) and 4-AP (100 μM) were applied for 3 min. Current-voltage values between the quinpirole and saline group were compared using a two-way ANOVA. The last minute of drug or saline application was normalized to the average of the 5-min baseline control period and these values are described as percent (%) of baseline under "Results." The voltage sensitivity of currents was estimated by measuring the membrane potential at which 50% of the maximal current was recorded and was compared between quinpirole and saline groups using a *t* test. To compare the effects of treatment (quinpirole, 4-AP, MTX *versus* saline) on normalized (% baseline) peak current values, a one-way ANOVA and Dunnett test for multiple comparisons was used. To explore the influence of Kv1.2 blockade on the ability of quinpirole to increase K$^+$ current, MTX was applied for 9 min and quinpirole was co-applied from minute 4 to 6 of the MTX incubation. To compare the effects of MTX preincubation on the influence of quinpirole *versus* saline, MTX, or quinpirole alone a one-way ANOVA with post hoc Newman Keuls pairwise comparisons was performed.

Immunoprecipitation and Western Blotting—COS-7 cells were cultured in Dulbecco's modified Eagle's medium/F-12 (Invitrogen) supplemented with 10% fetal bovine serum, 100 μg/ml of streptomycin, 100 IU/ml of penicillin, cells were grown at 37 °C in 5% CO$_2$. Cells were transfected with *D2S*, *D2L*, or *Kv1.2-YFP* (37) expression plasmids using FuGENE HD (Roche Applied Science) according to the manufacturer's instructions. 24 h after transfections cells were rinsed with cold PBS and mechanically disrupted using a cell scraper and a glass homogenizer and recovered in membrane extraction buffer (MEB; 125 mM KCl, 50 mM Tris-HCl, pH 7.5, 5 mM EDTA, pH 8.0) and protease and phosphatase inhibitor mixtures. Immunoprecipitation (IP) and Western blotting were performed as described elsewhere (38). Briefly, protein samples (400 μg) were pre-cleared via incubation with protein A/G-agarose (Invitrogen) for 2 h. Upon removal of agarose beads, cell lysates were probed using a mouse monoclonal antibody (4H6-7-3) directed against D2R (5 μg) overnight at 4 °C with agitation. Control samples were incubated with normal mouse IgG (5 μg). IP was performed by adding 20 μl of protein A/G-agarose slurry followed by a 3-h incubation at 4 °C with agitation. The beads were collected via centrifugation, washed three times with MEB, and then resuspended in Laemmli sample buffer. For Western blotting, proteins separated by denaturing 10% SDS-PAGE were transferred onto polyvinylidene difluoride membranes (Millipore). Membranes were blocked in 5% nonfat dry milk in PBS, 0.05% Tween 20 and incubated with either anti-Kv1.2 antibody (Alomone Labs) or anti-D2 dopamine receptor antibody (made in-house and previously characterized (38) and anti-actin antibody. For detection, membranes were incubated with HRP-conjugated secondary antibodies (Jackson ImmunoResearch Laboratories). Immunoblots were visualized using a chemiluminescent HRP substrate (Immobilon Western, Millipore).

For experiments with striatal tissue, mice were killed by cervical dislocation, after which the left and right hemistriata were rapidly dissected on an ice-cold surface and homogenized in MEB buffer with protease inhibitors (as above). Striatal synaptosomes were prepared according to a previously described procedure (39). The rest of the IP procedure was as for COS-7 cell extracts.

RESULTS

mRNA Expression Profiles in Acutely Dissociated Midbrain DA Neurons Demonstrate the Presence of Kv1.1, -1.2, -1.3, -1.4, and -1.6—To determine whether Kv1.1–1.6 subunits are present in DA neurons we first sought to detect their respective mRNA via multiplex RT-PCR from SN/VTA DA neurons purified by fluorescence-activated cell sorting from TH-eGFP mice. As evidence that GFP-sorted cells were dopaminergic and did not contain GABA neurons, we detected TH but not glutamic acid decarboxylase (GAD) mRNA in FACS-purified samples (Fig. 1*A*). We still detected GAD in mRNA extracted from whole midbrain (Fig. 1*B*) and in cells excluded from the sorted pool by their lack of GFP fluorescence (Fig. 1*C*). As shown in Fig. 1, Kv1.1, -1.2, -1.3, -1.4, and -1.6 but not Kv1.5 mRNA was expressed in FACS-purified DA neurons. The same mRNA expression profiles for Kv1.1–1.6, TH, and GAD were found in the five independent experiments using different cell samples. As a negative control we also assessed the presence of mRNA for Kv4.2, a member of the *Shal* voltage-gated K$^+$ channel subfamily with ubiquitous expression in brain (40), but absent from midbrain DA neurons (41). In 4 of 5 experiments, Kv4.2 could not be detected in FACS-purified DA neurons, whereas a weak signal for Kv4.2 was observed in one experiment performed with FACS samples derived from the youngest mice (P25; data not shown). As a positive control, the PCR product for all primers sets, including Kv1.5 and Kv4.2, were observed in midbrain (Fig. 1*B*) and mixed brain samples (data not shown). Kv1.5 and Kv4.2 were also detected in FACS-negative samples (Fig. 1*C*).

Immunocytochemical Expression of Kv1.1, -1.2, -1.3, -1.4, and -1.6 in Cultured DA Neurons—Immunolabeling was used to confirm Kv1 subunit expression in cultured DA neurons of the SN/VTA. Double immunofluorescence on primary DA cultures was performed using monoclonal antibodies against the DAT, to identify dopaminergic processes, and Kv1.1–1.6. As illustrated in Fig. 2, Kv1.1, -1.2, -1.3, -1.6, and, to a lesser extent, Kv1.4 subunits are localized to DA neurons of the SN/VTA, with the signal being particularly concentrated in axonal-like processes. In contrast, only a nonspecific signal (not above background level; supplemental Fig. S2) for Kv1.5 was detected, in agreement with the lack of Kv1.5 mRNA in the purified DA neuron preparations.

Localization of Kv1.1, -1.2, and -1.6 on Dopamine Axon Fibers—As Kv1.1, -1.2, -1.3, and -1.6 mRNA and protein expression
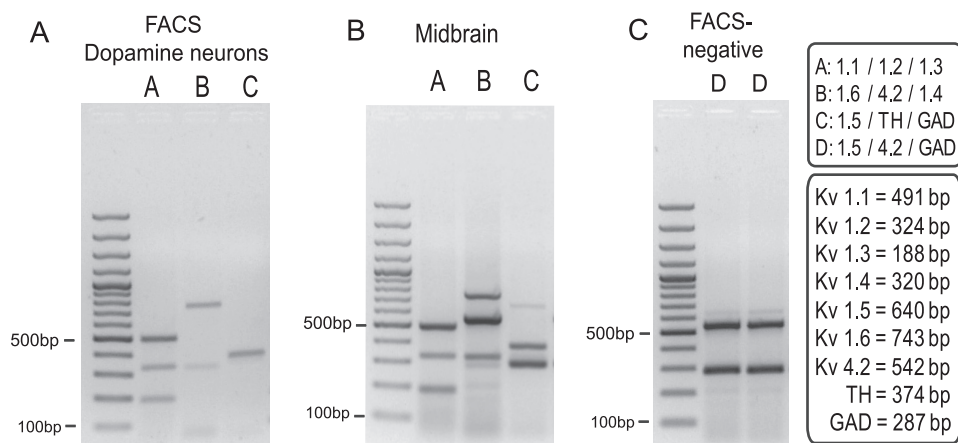
FIGURE 1. **Kv1 channels mRNA expression in DA neurons.** *A*, DA neurons of the SN/VTA isolated by FACS express Kv1.1, -1.2, -1.3, -1.4, and -1.6 mRNA, but not Kv1.5, Kv4.2, and GAD. *B*, presence of Kv1.1–1.6 and Kv4.2 mRNA in mRNA extracted from whole midbrain dissections. *C*, control, FACS-negative cells, express GAD and Kv4.2 mRNA.

were evident in FACS-purified DA cells and primary DA cultures, we next established whether or not these particular subunits are present on dopaminergic axons in the dorsolateral striatum, a region densely innervated by DA neurons. Although expression of Kv1.4 was observed in DA neuronal cultures, its level was low compared with other subunits examined and therefore its analysis was not further pursued in striatal slices. As shown in Fig. 3, double immunolabeling for DAT and Kv1.1, -1.2, -1.3, or -1.6 in striatal slices revealed the presence of Kv1.1, -1.2, and -1.6 on DAT-positive axons and/or axonal-like varicosities. Although we detected Kv1.3 immunoreactivity in slices, co-staining on DAT-positive axons was similar to that obtained in control experiments without primary antibody.

4-Aminopyridine Blocks the Ability of a D2 Agonist to Inhibit DA Overflow—To determine the role of Kv1 channels in D2-AR-mediated regulation of axonal DA overflow, we measured stimulation-evoked DA overflow in striatal slice preparations using fast scan cyclic voltammetry. Peak DA current values obtained from background-subtracted voltammograms (Fig. 4A) were plotted over time and show the time course of DA release and reuptake (Fig. 4, *B* and *C*). All subsequent voltammetry data are presented as normalized concentration values (normalized to the respective baseline control period). Under the conditions used, DA overflow was sensitive to tetrodotoxin treatment and thus activity dependent (data not shown).

As illustrated by Fig. 4D, basal stimulation-evoked DA overflow was stable between stimulations while decreasing slightly over time, resulting in a mean rundown of 10.2% after 30 min (89.79 ± 2.54; $n = 12;5$). Bath application of the D2 agonist, quinpirole (1 μM), inhibited DA overflow by 65% (35 ± 2.71; $n = 9;5$) (Fig. 4, *C* and *D*). In separate experiments, slices were incubated with 4-AP, a broad spectrum Kv1 channel blocker. We chose a 100 μM dose of 4-AP for its previously reported ability to block Kv1 (1.1, 1.2, 1.3, 1.5, 1.7, and 1.8) and Kv3 channels (3.1, 3.2, and 3.3) without blockade of the Kv2 and Kv4 subfamilies (42, 43). Previous evidence from our laboratory indicates that Kv3.1, -3.2, and -3.4 channel blockers fail to mod-

ulate D2-AR regulation of DA overflow.[5] Bath application of 4-AP alone increased DA overflow up to 180% relative to controls (160.52 ± 9.4 *versus* 91.9 ± 1.8; $t_{(5)} = 7.65$, $p < 0.001$) (Fig. 4F). The maximal effect of 4-AP on DA overflow was achieved after 16 min of application and remained stable at this elevated level (data not shown). Therefore, in separate experiments we preincubated slices for 20 min with 4-AP to examine whether this blocks the actions of quinpirole on DA overflow. 4-AP pre-incubation significantly attenuated the effect of quinpirole on DA overflow (Fig. 4, *C* and *D*). As shown in Fig. 4D, 4-AP inhibited the effect of quinpirole by 44.2% relative to quinpirole alone (63.75 ± 3.04 *versus* $35 \pm 2.71\%$; $t_{(13)} = 6.9$, $p < 0.001$).

Block of D2-AR-induced Inhibition of DA Overflow by Kv1 Subunit-specific Toxins—To characterize the Kv1 subtypes responsible for D2-AR regulation of DA overflow, we exploited several specific toxins for Kv1 channels that have been isolated from scorpion and snake venoms (44, 45). α-Dendrotoxin (αDTX) (from *Dendroaspis angusticeps*) blocks K$^+$ channels containing Kv1.1, Kv1.2, or Kv1.6 subunits, whereas dendrotoxin-K (DTX-K) (from *Dendroaspis polylepis*) specifically blocks Kv1.1-containing channels (45–47). We also tested two more recently described toxin blockers: maurotoxin (MTX) (from scorpio *Maurus palmatus*) and Osk-1 (from *Orthochirus scrobiculosus*). At the 10 nM dose used, MTX potently blocks Kv1.2-containing channels (48), whereas Osk-1 at 2 nM is a specific blocker of most Kv1.3 channels (49). Only one subunit of the channel is required for the binding of toxins, thus these toxins are able to block heteromeric channels containing at least one toxin-sensitive subunit (50). We investigated bath pre-application of each toxin for 25–30 min on the ability of quinpirole to inhibit DA overflow. At time-matched control conditions, the effect of quinpirole alone was determined 30 min after baseline DA overflow measurements. Quinpirole reduced DA overflow by 83.64% ($16.36 \pm 1.2\%$ of baseline values). As illustrated in Fig. 4E, blockade of combined Kv1.1, -1.2, and -1.6 subunit-containing channels by αDTX (100 nM) attenuated the inhibitory actions of quinpirole on evoked DA over-
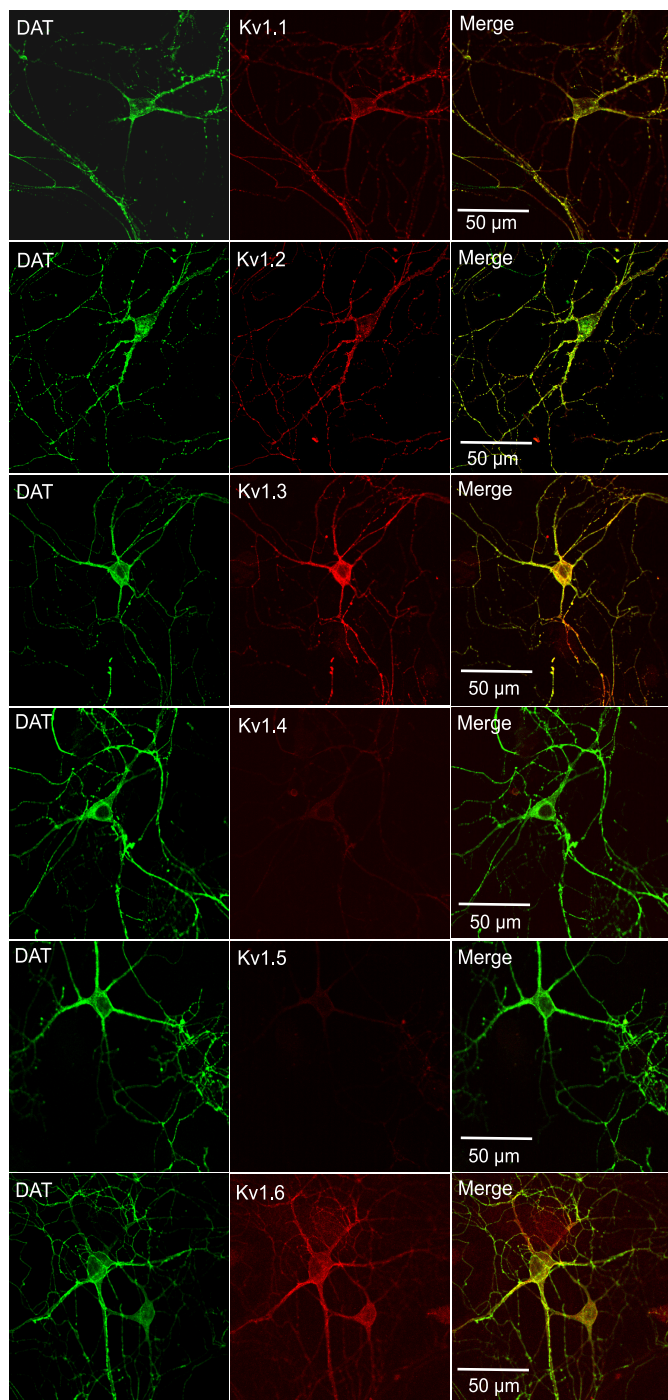

FIGURE 2. **Kv1.1, -1.2, -1.3, -1.6, and, to a lesser extent, Kv1.4 protein is expressed in cultured dopamine neurons.** $\times 60$ confocal images of mature dopamine cultures showing immunocytochemical colocalization of DAT (*green*) and Kv1.1, -1.2, -1.3, and a weak expression of Kv1.4 (*red*). Control experiments with secondary antibody alone are shown under supplemental "Experimental Procedures."

flow by 48.8% relative to slices treated with quinpirole alone (57.16 ± 7.4 *versus* $16.36 \pm 1.2\%$ of baseline values; $p < 0.001$) (overall $F_{(7,43)} = 8.863$; $p < 0.001$). Blockade of Kv1.2-containing channels with MTX produced the greatest effect of any subunit-specific toxin: MTX blocked 39.1% of the inhibitory action of quinpirole on DA overflow (49.01 ± 2.8 *versus* $16.36 \pm 1.2\%$; $p < 0.001$. Pre-application of DTX-K (Kv1.1 blocker)

diminished the effect of quinpirole on DA overflow by 30.8% (42.14 ± 2.8 *versus* $16.36 \pm 1.2\%$; $p < 0.001$). Finally, the Kv1.3 blocker, Osk-1, failed to significantly alter the ability of quinpirole to reduce the evoked DA overflow (29.39 ± 2.6 *versus* $16.36 \pm 1.2\%$; not significant). MTX was the only toxin blocker that increased DA overflow relative to basal rundown (Fig. 4*F*; 108.5 ± 7.4 *versus* $89.79 \pm 2.5\%$) (overall $F_{(6,45)} = 5.65$; $p < 0.05$). These findings suggest that Kv1.1, -1.2, and perhaps -1.6 subunit-containing channels mediate the inhibition of DA overflow by D2-AR activation. A particular role for the Kv1.2 subunit is underscored by our data demonstrating robust effects of Kv1.2 blockade to reduce the D2-AR-mediated inhibition of DA overflow and increase basal DA overflow.

D2-AR Inhibition of DA Overflow Is Diminished in Kv1.2$^{-/-}$ Knock-out Mice—To further investigate the contribution of Kv1.2 to D2-AR regulation of DA overflow, we assessed stimulation-evoked DA overflow in acute slice preparations from Kv1.2$^{-/-}$ mice and Kv1.2$^{+/+}$ wild type controls. As shown in Fig. 5, *A* and *B*, basal DA overflow was significantly higher in Kv1.2$^{-/-}$ mice relative to controls (195.0 ± 39.40 *versus* 100.0 ± 12.04; $t_{(10)} = 2.31$, $p < 0.05$). In addition, the effect quinpirole (1 μM) on DA overflow was significantly reduced in Kv1.2$^{-/-}$ mice relative to wild type controls (36.7 ± 3.26 *versus* 24 ± 6.03; $t_{(10)} = 1.86$; $p < 0.05$) (Fig. 5, *C* and *D*). These results corroborate our toxin data and provide evidence for a physiologically relevant effect of Kv1.2 activity in axonal D2-AR regulation of DA overflow.

Co-immunoprecipitation of D2-AR and Kv1.2—To begin exploring a potential interaction between D2-AR and Kv1.2, we evaluated whether Kv1.2 could co-immunoprecipitate with the D2 receptor. We first co-expressed YFP-tagged *Kv1.2* with *D2S* and *D2L* expression vectors in COS cells. Kv1.2 could indeed be immunoprecipitated with a D2 receptor antibody in both D2S- and D2L-expressing cells (Fig. 6*A*). To validate this finding, we also examined mouse striatal tissue and found that Kv1.2 was again reliably immunoprecipitated (Fig. 6*B*). Furthermore, the signal was absent in tissue extracts obtained from D2 KO mice (26) but present in extracts prepared from D2L KO mice, thus confirming the interaction with D2S, the isoform previously suggested to act as the main D2-AR (11). To further distinguish between pre- and postsynaptic D2 receptors, we also prepared striatal synaptosomes, a preparation highly enriched in axon terminals. We found that Kv1.2 could also be immunoprecipitated from this material (Fig. 6*C*). These findings suggest that Kv1.2 and D2-AR are components of a common signaling complex at the membrane.

Quinpirole Increases K$^+$ Conductance in D2-AR/Kv1.2 Cotransfected Cells—We next focused our attention on the functional interaction of the D2-AR and Kv1.2. As we were unable to measure a Kv1.2, MTX-sensitive current in the cell body of cultured midbrain DA neurons (data not shown), we assessed the functional coupling of D2-AR and Kv1.2 in transfected HEK293 cells. We measured the regulation of K$^+$ currents by the D2-AR in cells co-transfected with YFP-tagged *Kv1.2* and myc-tagged *D2S* (short isoform of the D2 receptor). Visualization of YFP fluorescence guided the selection of cells for whole cell patch clamp recordings. Counting of YFP (Kv1.2) and myc
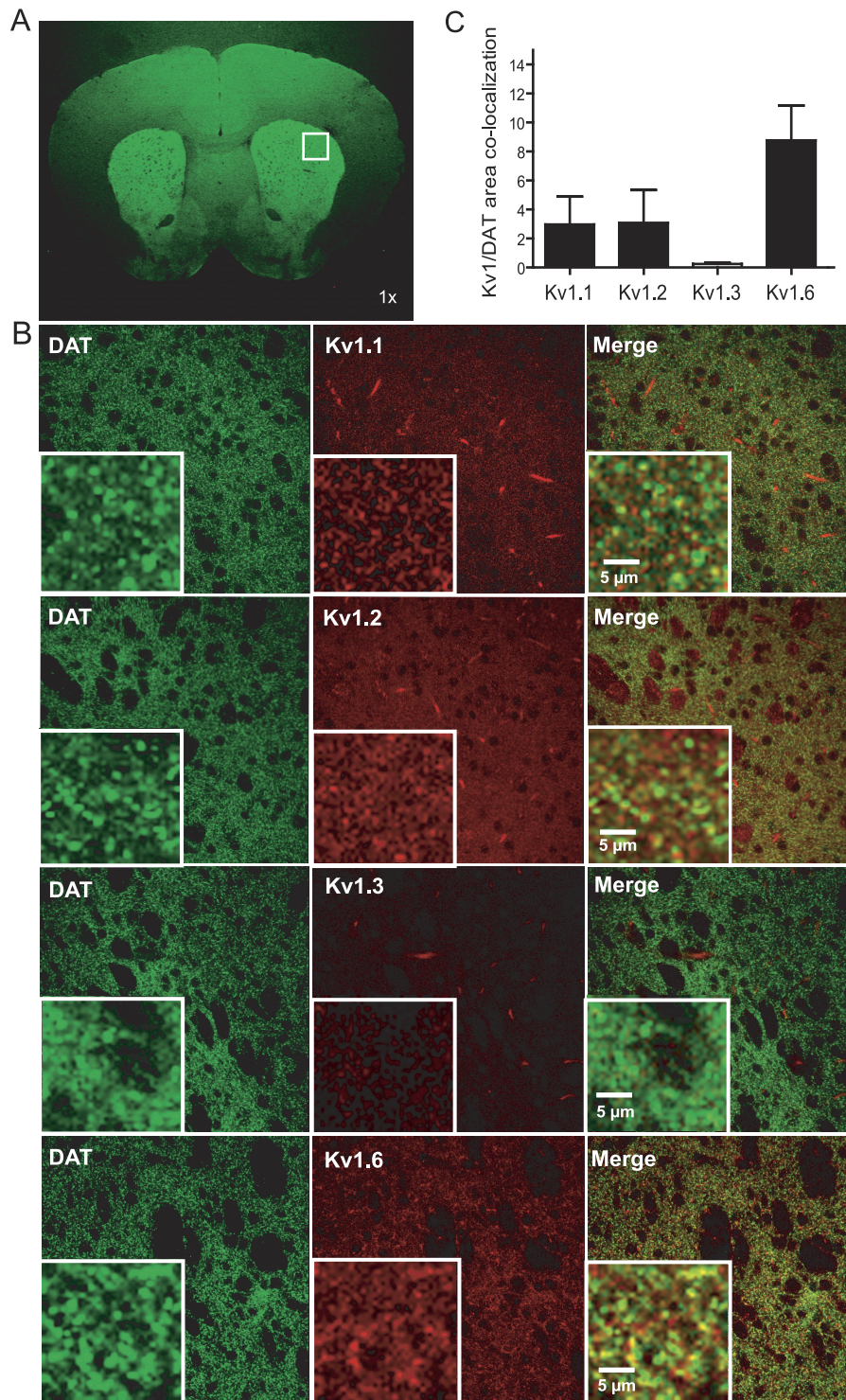
FIGURE 3. **Presynaptic localization of Kv1.1, -1.2, -.3, and -1.6 on dopamine axons of the dorsal striatum.** *A*, $\times$1 photomicrograph of DAT immunofluorescence in a striatal slice. The *box* identifies the region where $\times$40 confocal images were captured. *B*, $\times$40 confocal images with $\times$400 inserts demonstrating the presence of Kv1.1, -1.2, and -1.6 protein on DAT immunopositive axon terminals in the dorsal striatum. Kv1.3 immunostaining was near absent on DAT-positive fibers. *C*, area proportion of DAT-positive axonal fibers expressing Kv1.1, -1.2, -1.3, and -1.6 subunits (mean $\pm$ S.E.).

(D2S) immunolabeled cells revealed that the vast majority (84.9%) of Kv1.2-positive cells were indeed co-transfected with *D2S* (Fig. 7*A*). Cells were maintained at -80 mV and currents were recorded under voltage-clamp in response to sequences of depolarizing steps between -80 and $+30$ mV (Fig. 7*B*). As illustrated by the conductance-voltage curves in Fig. 7*B*, depolariza-

tions to values more positive than -40 mV were required to generate detectable currents in *Kv1.2-* and *D2S*-transfected cells. In contrast, currents only started to appear at 0 mV in non-transfected cells and with more than 10-fold lower amplitudes (data not shown). In both quinpirole- and saline-treated groups, the conductance amplitude increased in a voltage-de-
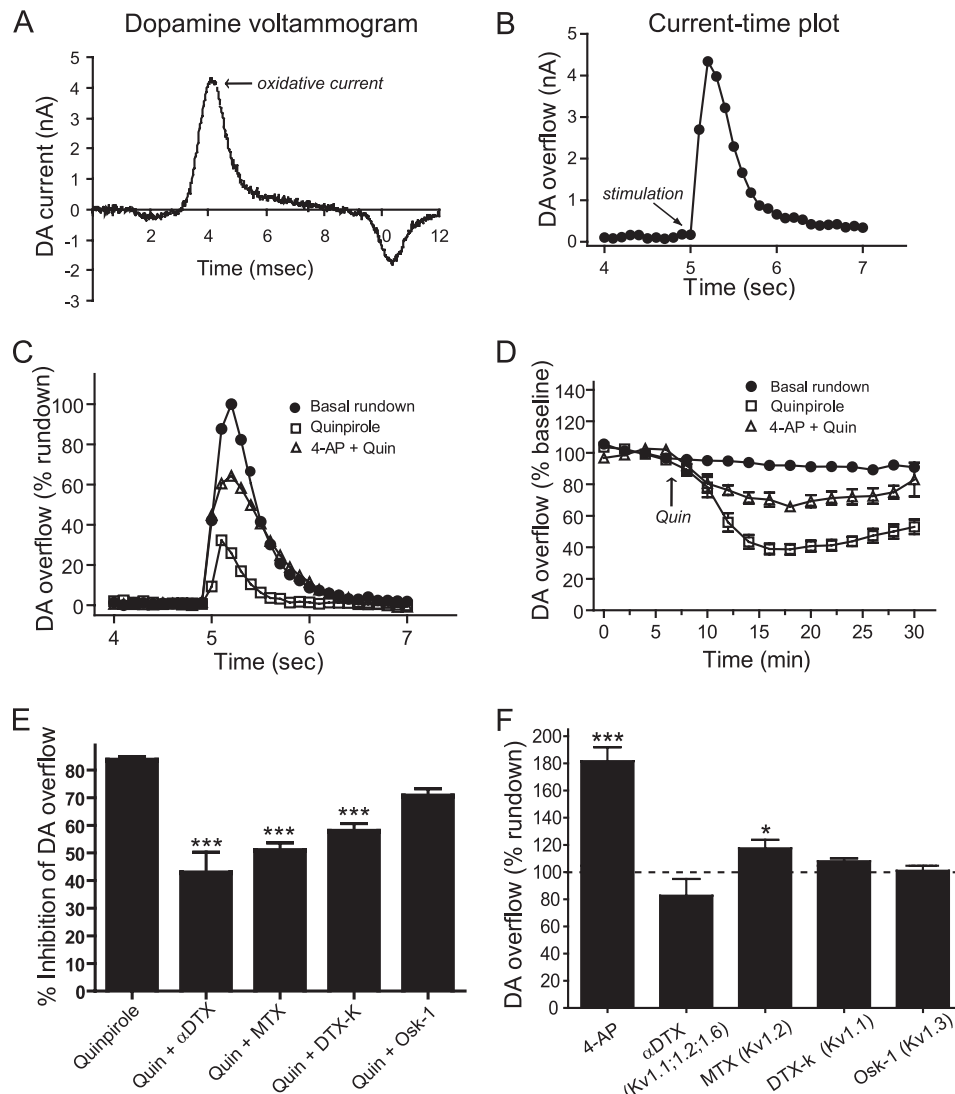
FIGURE 4. **Kv1 channel blockade reduces the ability of the D2 agonist quinpirole to decrease DA overflow.** *A*, representative background-subtracted cyclic voltammogram depicting oxidation and reduction current peaks for DA. Oxidative currents were obtained between ~300 and 500 mV (*versus* Ag/AgCl) corresponding to ~3.5–4.5 ms in the voltage waveform. *B*, current-time plot illustrating subsecond stimulation-evoked DA release and reuptake. *C*, current-time plots showing the influence of the D2 agonist, quinpirole (1 μM), and quinpirole in the presence of the broad spectrum Kv1 blocker, 4-AP (100 μM), on DA overflow (normalized to basal DA concentrations). *D*, time-course of DA overflow (plot of maximal overflow values (*B*) normalized to a pre-drug baseline control period). Quinpirole (1 μM; n = 9;5) inhibited DA overflow, whereas 4-AP (100 μM; n = 6;3) attenuated the effect of quinpirole to inhibit DA overflow. *E*, effect of preincubation with 4-AP (100 μM), α-DTX (100 nM; n = 4;4), a Kv1.1, -1.2, and -1.6 blocker, MTX (10 nM; n = 7;4), a specific Kv1.2 blocker, DTX-K (20 nM; n = 6;4), a specific Kv1.1 blocker; and Osk-1 (2 nM; n = 4;3), a specific Kv1.3 blocker, on the ability of quinpirole (1 μM) to inhibit DA overflow relative to controls with quinpirole alone (n = 6;4). *F*, effect of 4-AP (n = 6;3) and toxins alone on DA overflow relative to rundown (n = 11;6). Mean $\pm$ S.E.: *, $p < 0.05$; **, $p < 0.01$; ***, $p < 0.001$.

pendent manner. Activation of D2-AR (D2S) with quinpirole increased K$^+$ currents relative to cells treated with saline ($F_{(1,11)}$ = 26.5; $p < 0.0001$). A shift in voltage dependence was also induced by quinpirole: voltage at 50% maximal conductance was -0.82 ± 1.7 mV (mean $\pm$ S.E.) in control cells and -16.1 ± 1.9 mV in quinpirole-treated cells ($p < 0.0001$) (Fig. 7*C*). As shown in Fig. 7*D*, the wide spectrum Kv1 blocker, 4-AP (100 μM), reduced K$^+$ currents relative to saline-treated control (54.83 ± 4.02 *versus* 83.66 ± 5.6, $p < 0.05$) as did the specific Kv1.2 blocker, MTX (43.6 ± 4.96 *versus* 83.66 ± 5.6, $p < 0.01$). Importantly, MTX preincubation completely blocked the current-activating effects of quinpirole (Fig. 7*E*) (37.36 ± 7.43 *versus* 71.76 ± 6.78 (saline), $p < 0.05$; 127.9 ± 10.50 (quinpirole), $p < 0.001$; 43.46 ± 4.96 (MTX), not significant). We also recorded

currents in HEK293 cells co-transfected with *D2L* (long isoform of the D2 receptor) and *Kv1.2* (Fig. 7*F*). Quinpirole increased current activation by 26% relative to saline controls (104.4 ± 10.42 *versus* 77.47 ± 3.530, $t_{(10)} = 2.45$, $p < 0.05$).

Blockade of G$\beta\gamma$ Signaling Diminishes D2-AR-induced Inhibition of DA Overflow and Prevents the Potentiation of K$^+$ Conductance by Quinpirole—To begin exploring the signaling mechanisms by which D2-AR activation may be coupled to the opening of Kv1 channels, we investigated D2-AR inhibition of DA overflow using voltammetry under conditions of G$\beta\gamma$ and G$\alpha_{i/o}$ blockade. To block G$\beta\gamma$ function, we introduced a FLAG-tagged TAT-G protein-coupled receptor kinase carboxyl terminus (GRKct) scavenger peptide into DA neurons. The effectiveness of this peptide to block G$\beta\gamma$ was validated in DA
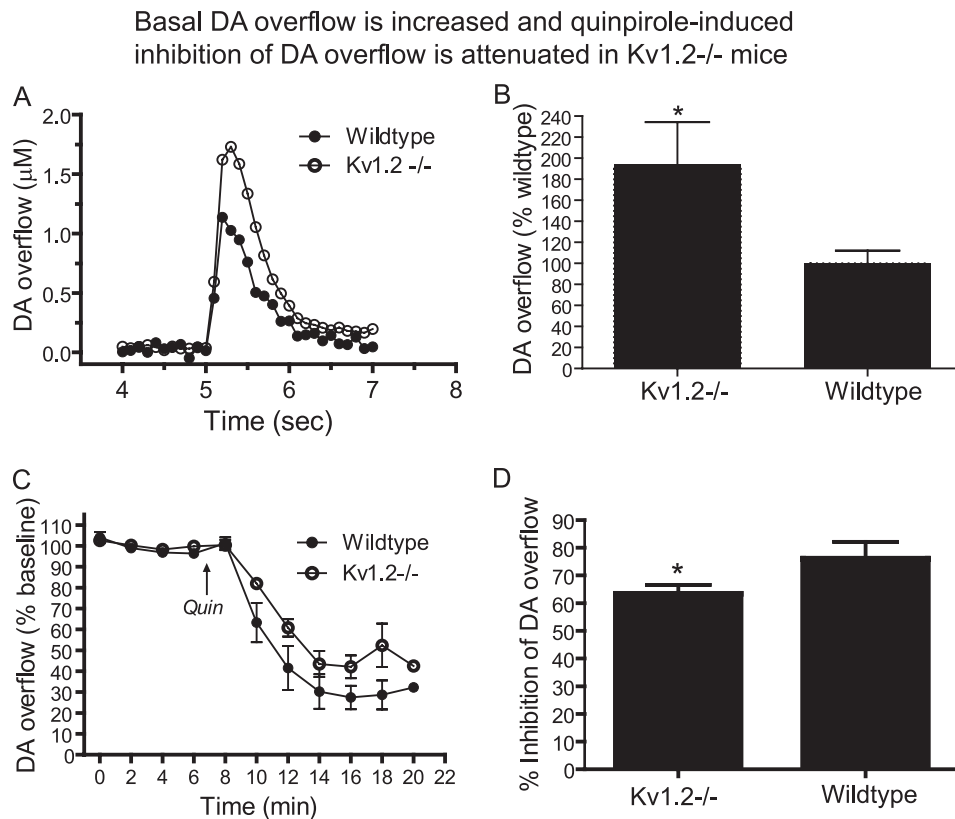
Basal DA overflow is increased and quinpirole-induced
inhibition of DA overflow is attenuated in Kv1.2-/- mice

FIGURE 5. **Basal DA overflow is potentiated, whereas D2-AR inhibition of DA overflow is diminished in Kv1.2$^{-/-}$ mice.** *A*, current-time plot illustrating increased stimulation-evoked DA overflow in a Kv1.2$^{-/-}$ mouse relative to a wild type control (Kv1.2$^{+/+}$). *B*, basal DA overflow is potentiated in Kv1.2$^{-/-}$ mice ($n = 6;3$) relative to wild type littermates ($n = 6;3$). *C*, reduced impact of quinpirole (1 μM) on stimulation-evoked DA overflow in Kv1.2$^{-/-}$ mice. Data depict DA overflow over time normalized to pre-drug baseline period. *D*, quinpirole-induced inhibition of DA overflow is attenuated in Kv1.2$^{-/-}$ mice ($n = 6;3$) relative to wild type littermates ($n = 6;3$) (mean $\pm$ S.E.; *, $p < 0.05$).
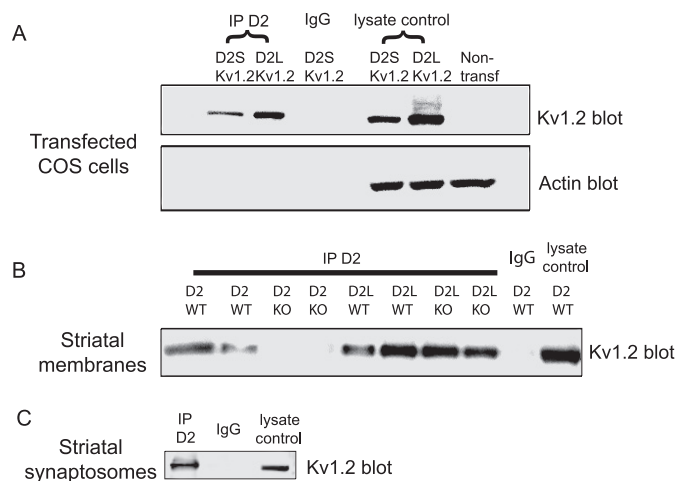

FIGURE 6. **Co-immunoprecipitation of D2S and Kv1.2.** *A*, immunoprecipitation of Kv1.2 by a D2 receptor antibody in protein extracts from COS cells transfected with *Kv1.2* and *D2S* or *D2L* (long-form of D2 receptor). Normal mouse IgG was used as a negative control. Protein extracts were used as positive control ("lysate control"). Demonstrating the specificity of the immunoprecipitation, actin was absent in D2-immunoprecipitated samples and negative control. *B*, immunoprecipitation of Kv1.2 by a D2 receptor antibody in mice striatal membrane protein extracts. No immunoprecipitation was obtained with normal mouse IgG or in extracts obtained from D2 KO mice, although Kv1.2 was immunoprecipitated from striatal extracts of D2L KO mice. *C*, immunoprecipitation of Kv1.2 by a D2 receptor antibody in synaptosome membrane protein extracts prepared from the striatum of mice.

cultures by assessing the ability of the peptide to attenuate D2-AR-induced inhibition of DA cell firing, a process known to rely on G$\beta\gamma$ coupling and activation of somato-dendritic G-protein gated inward-rectifying K$^+$ channels (supplemental Fig. S1*A*) (51). Furthermore, penetration of active and control peptides in striatal slices was validated by immunolabeling with anti-FLAG and anti-DAT antibodies (supplemental Fig. S1*B*). As shown in Fig. 8*A*, preincubation of slices with TAT-GRK peptide (1 μM) partially blocked the ability of quinpirole (1 μM) to inhibit stimulation-evoked DA overflow by 23.6% relative to the inactive peptide (1 μM) (54.9 $\pm$ 1.1 *versus* 71.78 $\pm$ 5.5; $p < 0.01$). NEM, a sulfhydryl alkalating agent, selectively reduces responses mediated by pertussis toxin-sensitive G proteins (G$_{i/o}$) (52). NEM was used to block G$_{i/o}$ because pertussis toxin requires long incubation times that are incompatible with the use of acute slice preparations. Pre-application of NEM (200 nM) blocked the inhibitory actions of quinpirole by 71.8% (23.6 $\pm$ 13.4 *versus* 83.6 $\pm$ 1.2; $p < 0.01$) (Fig. 8*B*). Finally, to determine the contribution of G$\beta\gamma$ signaling in the activation of Kv1.2 by D2-AR, we triple transfected HEK293 cells with *Kv1.2*, *D2S*, and *GRKct* (Fig. 8*C*) and recorded K$^+$ currents following saline or quinpirole (1 μM) application. As illustrated in Fig. 8*D*, the presence of GRKct completely prevented the previously described increase in K$^+$ conductance induced by quinpirole. These findings are consistent with the involve-
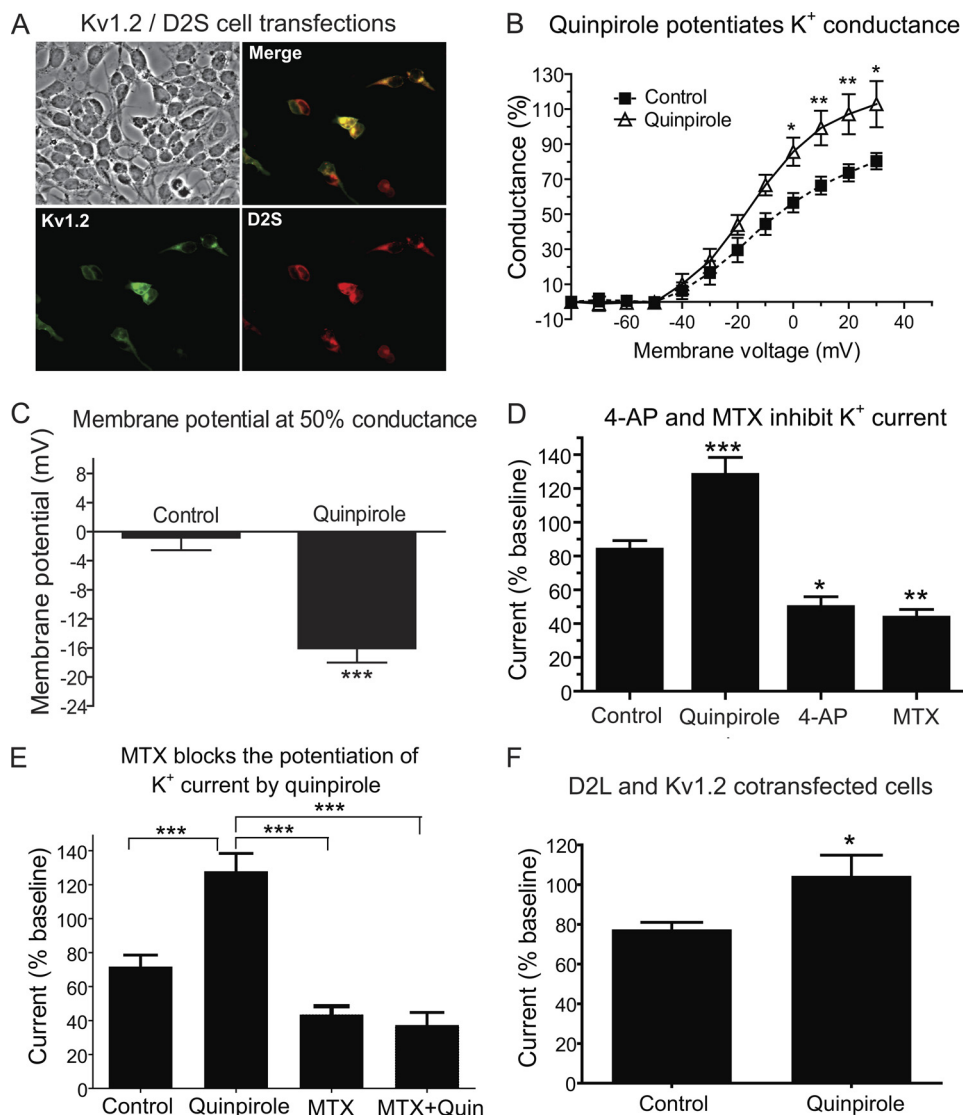
FIGURE 7. **Quinpirole increases K$^+$ conductance in *Kv1.2/D2S* co-transfected cells.** *A*, HEK293 cells co-transfected with Kv1.2 (*green*) and D2S (D2-AR) (*red*). *B*, application of the D2 agonist, quinpirole (1 μM; *n* = 10) to co-transfected cells increased K$^+$ conductance as compared with saline (*n* = 7). *C*, the membrane potential at 50% maximal conductance was substantially reduced by quinpirole *versus* saline. *D*, quinpirole increased maximum K$^+$ conductance, whereas the wide spectrum Kv1 blocker, 4-AP (100 μM; *n* = 9) and the Kv1.2 blocker, MTX (50 nM; *n* = 8), blocked a large proportion of the K$^+$ current *versus* saline control (*n* = 7). *E*, blocking Kv1.2 by preincubation with MTX (*n* = 8) prevented the increase in K$^+$ current by quinpirole. *F*, quinpirole (*n* = 6) potentiated the K$^+$ current in HEK cells co-transfected with *D2L* and *Kv1.2* as compared with saline (*n* = 6). Mean $\pm$ S.E.: *, $p < 0.05$; **, $p < 0.01$; ***, $p < 0.001$.

ment of $G\alpha_{i/o}$ signaling (53) in D2-AR-mediated inhibition of axonal DA release and provide new evidence suggesting that $G\beta\gamma$ proteins contribute to the coupling of axonal D2-AR and Kv1.2 activation leading to reduced DA overflow.

DISCUSSION

Identifying the mechanisms by which D2-AR regulates axonal DA release in the striatum has clear implications for understanding the motor, cognitive, and emotional functions tied to striatal DA signaling. In the present study, we demonstrate the importance of voltage-gated K$^+$ channels of the Kv1 subfamily in the actions of presynaptic D2-AR to regulate axonal DA overflow. In particular, by using Kv1.2$^{-/-}$ mice and a Kv1.2 toxin blocker during real time measures of DA release along with K$^+$ conductance measurements in Kv1.2-transfected cells, we reveal a specific role for Kv1.2 in D2-AR func-

tion. Collectively, our observations uncover a mechanism by which axonal D2-AR attenuates DA overflow by regulating the function of Kv1 channels and isolate the importance of Kv1.2 in this process by demonstrating the coupling of D2-AR to Kv1.2 channels.

Kv1.1 through 1.6 subunits are widely expressed in the mammalian brain where they act to regulate excitability and secretion. This study is the first to demonstrate Kv1 subunit expression in midbrain DA neurons. FACS-purified DA neuron preparations were probed for Kv1 subunit expression to reveal Kv1.1, -1.2, -1.3, -1.4, and -1.6 mRNA in DA neurons of the SN/VTA. Although Kv1.5 was observed in whole midbrain samples, it was not detected in purified DA samples, a finding that is consistent with the relatively low abundance of this subunit in neurons (54). Expression analyses at the RNA level largely match those obtained at the protein level as Kv1.1, -1.2,

A — Gβγ blockade attenuates quinpirole-induced inhibition of DA overflow

B — Gαi/o blockade attenuates quinpirole-induced inhibition of DA overflow

C — Kv1.2 / D2S / GRKct cell transfections

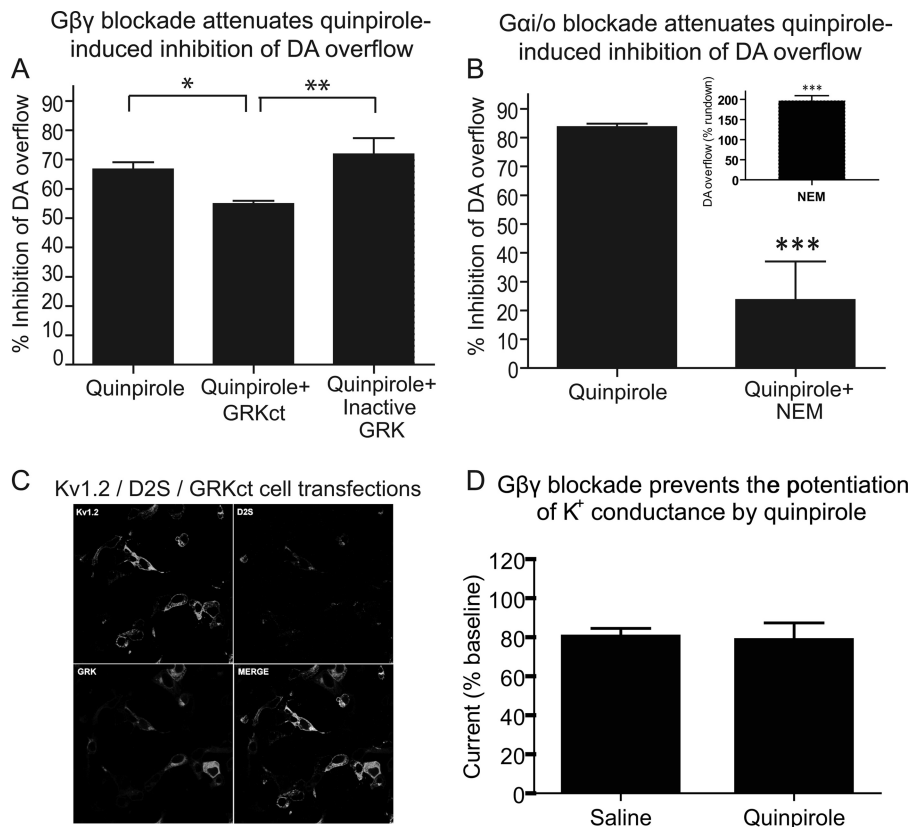D — Gβγ blockade prevents the potentiation of K$^+$ conductance by quinpirole

FIGURE 8. **Blocking Gβγ signaling decreases the ability of quinpirole to inhibit striatal DA overflow and prevents quinpirole-induced increases in K$^+$ current.** *A*, preincubation of striatal slices with the Gβγ scavenger peptide, active TAT-GRKct (1 μM; $n = 6;4$) attenuated the actions of quinpirole by 23.6% relative to the inactive peptide (1 μM; $n = 6; 3$). *B*, preincubation of striatal slices with NEM (200 nM; $n = 6;3$), a blocker of pertussis toxin-sensitive G$_{i/o}$ proteins, reduced the inhibitory actions of quinpirole by 71.8% relative to quinpirole alone (1 μM; $n = 6;4$). As shown by the *inset*, NEM alone increased basal DA overflow. *C*, HEK293 cells co-transfected with *Kv1.2* (*green*), *D2S* (*red*), and *GRKct* (*blue*). *D*, K$^+$ current measurements in triple transfected cells following saline or quinpirole (1 μM) application. Blocking Gβγ signaling by introducing GRKct prevents the increase in K$^+$ conductance by quinpirole. Mean ± S.E.: *, $p < 0.05$; **, $p < 0.01$; ***, $p < 0.001$.

-1.3, -1.4, and -1.6, but not Kv1.5, immunofluorescence was detected in cultured DA neurons. In all cases, Kv1 staining was observed along somatodendritic and axonal-like domains of DA neurons, which is consistent with Kv1 expression patterns described elsewhere and in the role of these channels in diverse cellular functions (19). Expression of each Kv1 subunit was apparent in all DAT-positive neurons, thus suggesting that these subunits are co-expressed in DA neurons. The Kv1 channel pore is composed of four α subunits that often co-assemble to form heteromultimeric channels (23, 24) and thus Kv1 subunits may combine in such a manner in DA neurons, although this remains to be specifically examined.

Immunohistochemical examination of striatal slices revealed Kv1.1, -1.2, and -1.6 along DA-positive axons and/or terminals. In contrast, Kv1.3 immunolabeling was near absent in DA processes. Kv1.2 is the most abundant subunit in the mammalian brain and is present in the great majority of Kv1 channel complexes and in all Kv1.1 and -1.6-containing channel complexes (55). The relative difference in the abundance of Kv1 subunits on DA-positive fibers that was measured is likely a close representation rather than a reflection of variations in antibody staining because immunolabeling of tubular microvasculature-like structures was similar across subunits (not shown). Moreover, the specific binding and labeling of the Kv1 antibodies used has been validated (56). Kv1 channels are reported to be

predominantly localized to the immediate presynaptic region of axon terminals (54). It may be considered likely that Kv1.1, -1.2, and -1.6 subunits are thus also preferentially localized to the immediate presynaptic region of DA neurons. However, the amount of DAT and Kv1 co-localization we observed in striatal slices was relatively small: our images may have underestimated the true level of co-localization, because in a given confocal image plane, we would expect the number of DA axons coursing through and terminating at sites more rostral or caudal to exceed the number of presynaptic DA terminals regions. The precise location of Kv1 channels on DA axons will require additional experimentation including electron microscopy. Taken together, the expression data provide strong evidence for the presence of Kv1.1, -1.2, and -1.6 subunit-containing channels in DA neurons and their localization on nigrostriatal dopaminergic axons and/or axon terminals.

Real time measurement of DA overflow with cyclic voltammetry provides an ideal tool to directly assess the functional contribution of Kv1 channels in D2-AR regulation of DA overflow. Moreover, the use of acute slice preparations for DA concentration measurements permits precise spatial and temporal control for the application of multiple drugs/toxins. Preincubation of slices with αDTX, a blocker of Kv1.1, -1.2, and -1.6 subunit-containing channels, blocked approximately half of the effect of quinpirole on evoked DA overflow. Interestingly, the

influence of αDTX on D2-AR-mediated inhibition (48.8% block) was similar in magnitude to that obtained with the broad spectrum Kv1 blocker, 4-AP (44.2% block; Fig. 4D). Although 4-AP can also block Kv3-containing channels and a recent report implicates voltage-activated Ca^{2+} channel facilitation (57), our results with αDTX suggest that the effects of 4-AP specifically on D2-AR function may be mostly due to its actions to block Kv1.1, -1.2, and -1.6.

Despite evidence of Kv1 channel involvement, 4-AP did not fully block the actions of the quinpirole to reduce DA overflow, suggesting that additional mechanisms mediate the ability of the D2-AR to inhibit DA overflow. One possibility is that D2-AR-mediated inhibition of axonal overflow is also mediated in part by other mechanisms such as direct inhibition of exocytosis or inhibition of voltage-dependent Ca^{2+} channels in terminals. In support of the first of these mechanisms, previous work in cultured DA neurons suggests that D2-AR can negatively regulate the secretory process at a step that is downstream to calcium influx in axon terminals (16). However, DA release was not directly measured in that study and the possible implication of calcium channel inhibition was also not directly examined.

Our results establish a particular role for Kv1.2 channels in the regulation of DA release as MTX had the greatest impact of any of the Kv1 subunit-specific toxins to block the inhibiting actions of quinpirole on DA overflow. Additionally, we found that blockade of Kv1.1 with DTX-K diminished the influence of quinpirole on evoked DA overflow. In contrast, pre-treatment of slices with Osk-1, a Kv1.3 blocker, was without effect on DA overflow. Interestingly, both αDTX and DTX-K did not increase basal DA overflow, whereas MTX slightly enhanced it. These results may be taken to suggest a more defined role of Kv1.1, -1.2, and -1.6 channel activation in the regulation of DA release by D2-AR. On the contrary, 4-AP substantially increased basal DA overflow. It is not clear why this effect was not mimicked by αDTX, however, we reason that this could be due to the ability of 4-AP to additionally facilitate the opening of voltage-activated Ca^{2+} channels (57). Altogether, these data support our immunohistochemical findings suggesting that Kv1.1, Kv1.2, and possibly Kv1.6 subunit-containing channels mediate the regulation of DA overflow operated by D2-AR.

The role of Kv1.2 in striatal DA overflow and D2-AR regulation of axonal DA overflow was substantiated in $Kv1.2^{-/-}$ mouse knock-out experiments. Basal DA overflow was significantly elevated in $Kv1.2^{-/-}$ mice, whereas the effect of quinpirole on DA overflow was significantly attenuated in $Kv1.2^{-/-}$ mice relative to controls. These data corroborate those obtained with pharmacological blockade of Kv1.2. That functional deficits were detected in the $Kv1.2^{-/-}$ mice imply that Kv1.2 is a critical regulator of DA release and D2-AR regulation of DA release, perhaps through D2R-mediated regulation of the voltage sensitivity of presynaptic Kv1 channels.

To determine whether D2-AR and Kv1.2 might be part of the same complex, we carried out IP experiments and patch clamp recordings of K^+ currents. Our IP data from transfected cells and striatal membrane and synaptosomal preparations suggest that D2-AR and Kv1.2 proteins are part of a common signaling complex implicating D2-AR in dopaminergic axon terminals.

Furthermore, we measured the ability of quinpirole to regulate K^+ channel conductance in cells co-transfected with *Kv1.2* and D2-AR (*D2S*). D2-AR activation substantially increased K^+ conductance in a voltage-dependent manner. Moreover, the increase in conductance by quinpirole was fully blocked by the Kv1.2 channel blocker, MTX. Collectively, these data directly demonstrate the contribution of Kv1.2 to D2-AR activation. The voltage sensitivity of Kv1.2 was enhanced in response to D2-AR activation, thus identifying a possible mechanism underlying the enhancement of K^+ currents.

Providing insight into the G protein signals that may mediate the interaction between D2-AR and Kv1.2, we found that a peptide inhibitor of Gβγ diminished the inhibitory effect of quinpirole on striatal DA overflow. In addition, our K^+ current measurements in cells show that blocking Gβγ by introducing a GRKct construct prevents the increase in K^+ current produced by quinpirole. Although further work will be required to elucidate the details of the function and organization of this complex, these experiments suggest that Gβγ and Kv1.2 interact. Nonetheless, whether the regulation of Kv1.2 by D2-AR involves other effectors (58, 59), or other direct or indirect interactions between D2-AR, Kv1.2, and G-proteins remains to be determined. The modest efficacy of the GRKct in reducing the inhibitory effect of quinpirole on DA overflow stands in contrast with the complete block of Kv1.2 channel regulation with this same peptide. This could result from insufficient accumulation of the TAT-delivered peptide in the brain slice preparation. In comparison, high levels of the peptide were produced in HEK293 cells following transfection. To summarize, the expression of Kv1.1, -1.2, and -1.6 in DA neurons and localization to axon terminals, along with the ability of subunit-selective channel blockers to attenuate D2-AR inhibition of DA overflow implicate Kv1.1, -1.2, and -1.6 in D2-AR regulation of striatal DA release. By means of both pharmacological and genetic Kv1.2 loss-of-function, a particular role was underlined for Kv1.2 in the modulation of axonal DA overflow by D2-AR. Furthermore, we show that direct activation of D2-AR increases Kv1.2 conductance in co-transfected cells and that a Kv1.2 blocker prevents this effect, an effect that may be due to heightened voltage sensitivity of Kv1.2 channels. Co-IP experiments argue that D2-AR and Kv1.2 are part of a common signaling complex, compatible with the physiological interaction that we observed. We hypothesize that D2-AR activation decreases DA release in part by facilitating the voltage-dependent opening of Kv1.2-containing channels by a Gβγ-dependent mechanism, thus potentially leading to a shunting of axon terminal depolarization and secondary reduction in Ca^{2+} influx and DA exocytosis. Collectively, this work adds Kv1.2 activation to the processes that mediate the plasticity of DA release and offers a novel mechanism by which DA release may be impaired in pathophysiological and neurological conditions.

REFERENCES

1. Volkow, N. D., Wang, G. J., Fowler, J. S., Logan, J., Gatley, S. J., Hitzemann, R., Chen, A. D., Dewey, S. L., and Pappas, N. (1997) *Nature* **386,** 830–833

2. Fulton, S., Pissios, P., Manchon, R. P., Stiles, L., Frank, L., Pothos, E. N., Maratos-Flier, E., and Flier, J. S. (2006) *Neuron* **51,** 811–822

3. Geiger, B. M., Behr, G. G., Frank, L. E., Caldera-Siu, A. D., Beinfeld, M. C., Kokkotou, E. G., and Pothos, E. N. (2008) *FASEB J.* **22,** 2740–2746

4. Carelli, R. M., and Wightman, R. M. (2004) *Curr. Opin. Neurobiol.* **14,** 763–768

5. Schultz, W., Dayan, P., and Montague, P. R. (1997) *Science* **275,** 1593–1599

6. Grace, A. A., Floresco, S. B., Goto, Y., and Lodge, D. J. (2007) *Trends Neurosci.* **30,** 220–227

7. Gonon, F. G., and Buda, M. J. (1985) *Neuroscience* **14,** 765–774

8. Werner, P., Hussy, N., Buell, G., Jones, K. A., and North, R. A. (1996) *Mol. Pharmacol.* **49,** 656–661

9. Inanobe, A., Yoshimoto, Y., Horio, Y., Morishige, K. I., Hibino, H., Matsumoto, S., Tokunaga, Y., Maeda, T., Hata, Y., Takai, Y., and Kurachi, Y. (1999) *J. Neurosci.* **19,** 1006–1017

10. Giros, B., Sokoloff, P., Martres, M. P., Riou, J. F., Emorine, L. J., and Schwartz, J. C. (1989) *Nature* **342,** 923–926

11. Usiello, A., Baik, J. H., Rougé-Pont, F., Picetti, R., Dierich, A., LeMeur, M., Piazza, P. V., and Borrelli, E. (2000) *Nature* **408,** 199–203

12. Dal Toso, R., Sommer, B., Ewert, M., Herb, A., Pritchett, D. B., Bach, A., Shivers, B. D., and Seeburg, P. H. (1989) *EMBO J.* **8,** 4025–4034

13. Lacey, M. G., Mercuri, N. B., and North, R. A. (1987) *J. Physiol.* **392,** 397–416

14. Cass, W. A., and Zahniser, N. R. (1991) *J. Neurochem.* **57,** 147–152

15. Pillai, G., Brown, N. A., McAllister, G., Milligan, G., and Seabrook, G. R. (1998) *Neuropharmacology* **37,** 983–987

16. Congar, P., Bergevin, A., and Trudeau, L. E. (2002) *J. Neurophysiol.* **87,** 1046–1056

17. Wang, H., Kunkel, D. D., Martin, T. M., Schwartzkroin, P. A., and Tempel, B. L. (1993) *Nature* **365,** 75–79

18. Sheng, M., Liao, Y. J., Jan, Y. N., and Jan, L. Y. (1993) *Nature* **365,** 72–75

19. Wang, H., Kunkel, D. D., Schwartzkroin, P. A., and Tempel, B. L. (1994) *J. Neurosci.* **14,** 4588–4599

20. Dodson, P. D., Billups, B., Rusznák, Z., Szűcs, G., Barker, M. C., and Forsythe, I. D. (2003) *J. Physiol.* **550,** 27–33

21. Rhodes, K. J., Strassle, B. W., Monaghan, M. M., Bekele-Arcuri, Z., Matos, M. F., and Trimmer, J. S. (1997) *J. Neurosci.* **17,** 8246–8258

22. Sheng, M., Tsaur, M. L., Jan, Y. N., and Jan, L. Y. (1992) *Neuron* **9,** 271–284

23. Deal, K. K., Lovinger, D. M., and Tamkun, M. M. (1994) *J. Neurosci.* **14,** 1666–1676

24. Sheng, M., Tsaur, M. L., Jan, Y. N., and Jan, L. Y. (1994) *J. Neurosci.* **14,** 2408–2417

25. Brew, H. M., Gittelman, J. X., Silverstein, R. S., Hanks, T. D., Demas, V. P., Robinson, L. C., Robbins, C. A., McKee-Johnson, J., Chiu, S. Y., Messing, A., and Tempel, B. L. (2007) *J. Neurophysiol.* **98,** 1501–1525

26. Baik, J. H., Picetti, R., Saiardi, A., Thiriet, G., Dierich, A., Depaulis, A., Le Meur, M., and Borrelli, E. (1995) *Nature* **377,** 424–428

27. Mendez, J. A., Bourque, M. J., Dal Bo, G., Bourdeau, M. L., Danik, M., Williams, S., Lacaille, J. C., and Trudeau, L. E. (2008) *J. Neurosci.* **28,** 6309–6318

28. Corpet, F. (1988) *Nucleic Acids Res.* **16,** 10881–10890

29. Jomphe, C., Bourque, M. J., Fortin, G. D., St-Gelais, F., Okano, H., Kobayashi, K., and Trudeau, L. E. (2005) *J. Neurosci. Methods* **146,** 1–12

30. Fasano, C., Thibault, D., and Trudeau, L. E. (2008) *Curr. Protoc. Neurosci.* **44,** 3.21.1–3.21.19

31. Rasband, W. J. (1997–2009) *ImageJ*, National Institutes of Health, Bethesda, MD, rsb.info.nih.gov/ij

32. Kawagoe, K. T., Zimmerman, J. B., and Wightman, R. M. (1993) *J. Neurosci. Methods* **48,** 225–240

33. Bath, B. D., Michael, D. J., Trafton, B. J., Joseph, J. D., Runnels, P. L., and Wightman, R. M. (2000) *Anal. Chem.* **72,** 5994–6002

34. Hochstetler, S. E., Puopolo, M., Gustincich, S., Raviola, E., and Wightman, R. M. (2000) *Anal. Chem.* **72,** 489–496

35. John, C. E., and Jones, S. (2006) in *Electrochemical Methods for Neuroscience* (Micheal, A. C., and Borland, L. M., eds) pp. 49–62, CRC Press, Boca Raton, FL

36. Crespo, P., Cachero, T. G., Xu, N., and Gutkind, J. S. (1995) *J. Biol. Chem.* **270,** 25259–25265

37. Williams, M. R., Markey, J. C., Doczi, M. A., and Morielli, A. D. (2007) *Proc. Natl. Acad. Sci. U.S.A.* **104,** 17412–17417

38. Tirotta, E., Fontaine, V., Picetti, R., Lombardi, M., Samad, T. A., Oulad-Abdelghani, M., Edwards, R., and Borrelli, E. (2008) *Cell Cycle* **7,** 2241–2248

39. Bouvier, D., Corera, A. T., Tremblay, M. E., Riad, M., Chagnon, M., Murai, K. K., Pasquale, E. B., Fon, E. A., and Doucet, G. (2008) *J. Neurochem.* **106,** 682–695

40. Birnbaum, S. G., Varga, A. W., Yuan, L. L., Anderson, A. E., Sweatt, J. D., and Schrader, L. A. (2004) *Physiol. Rev.* **84,** 803–833

41. Liss, B., Franz, O., Sewing, S., Bruns, R., Neuhoff, H., and Roeper, J. (2001) *EMBO J.* **20,** 5715–5724

42. Grissmer, S., Nguyen, A. N., Aiyar, J., Hanson, D. C., Mather, R. J., Gutman, G. A., Karmilowicz, M. J., Auperin, D. D., and Chandy, K. G. (1994) *Mol. Pharmacol.* **45,** 1227–1234

43. Coetzee, W. A., Amarillo, Y., Chiu, J., Chow, A., Lau, D., McCormack, T., Moreno, H., Nadal, M. S., Ozaita, A., Pountney, D., Saganich, M., Vega-Saenz de Miera, E., and Rudy, B. (1999) *Ann. N.Y. Acad. Sci.* **868,** 233–285

44. Tytgat, J., Chandy, K. G., Garcia, M. L., Gutman, G. A., Martin-Eauclaire, M. F., van der Walt, J. J., and Possani, L. D. (1999) *Trends Pharmacol. Sci.* **20,** 444–447

45. Harvey, A. L. (2001) *Toxicon* **39,** 15–26

46. Southan, A. P., and Robertson, B. (1998) *Br. J. Pharmacol.* **125,** 1375–1381

47. Wang, F. C., Bell, N., Reid, P., Smith, L. A., McIntosh, P., Robertson, B., and Dolly, J. O. (1999) *Eur. J. Biochem.* **263,** 222–229

48. Castle, N. A., London, D. O., Creech, C., Fajloun, Z., Stocker, J. W., and Sabatier, J. M. (2003) *Mol. Pharmacol.* **63,** 409–418

49. Mouhat, S., Visan, V., Ananthakrishnan, S., Wulff, H., Andreotti, N., Grissmer, S., Darbon, H., De Waard, M., and Sabatier, J. M. (2005) *Biochem. J.* **385,** 95–104

50. Hopkins, W. F. (1998) *J. Pharmacol. Exp. Ther.* **285,** 1051–1060

51. Davila, V., Yan, Z., Craciun, L. C., Logothetis, D., and Sulzer, D. (2003) *J. Neurosci.* **23,** 5693–5697

52. Shapiro, M. S., Wollmuth, L. P., and Hille, B. (1994) *J. Neurosci.* **14,** 7109–7116

53. Montmayeur, J. P., Guiramand, J., and Borrelli, E. (1993) *Mol. Endocrinol.* **7,** 161–170

54. Misonou, H., and Trimmer, J. S. (2004) *Crit. Rev. Biochem. Mol. Biol.* **39,** 125–145

55. Scott, V. E., Muniz, Z. M., Sewing, S., Lichtinghagen, R., Parcej, D. N., Pongs, O., and Dolly, J. O. (1994) *Biochemistry* **33,** 1617–1623

56. Rhodes, K. J., and Trimmer, J. S. (2006) *J. Neurosci.* **26,** 8017–8020

57. Wu, Z. Z., Li, D. P., Chen, S. R., and Pan, H. L. (2009) *J. Biol. Chem.* **284,** 36453–36461

58. Ramu, Y., Xu, Y., and Lu, Z. (2006) *Nature* **442,** 696–699

59. Tsai, W., Morielli, A. D., Cachero, T. G., and Peralta, E. G. (1999) *EMBO J.* **18,** 109–118